Letter

Supercurrent reversal in ferromagnetic hybrid nanowire Josephson junctions

D. Razmadze,[1,*] R. Seoane Souto,[1,2,*] L. Galletti,[1] A. Maiani,[1] Y. Liu,[1] P. Krogstrup,[1] C. Schrade,[1] A. Gyenis,[1,†] C. M. Marcus,[1] and S. Vaitiekėnas[1]

[1]*Center for Quantum Devices, Niels Bohr Institute, University of Copenhagen, 2100 Copenhagen, Denmark*
[2]*Division of Solid State Physics and NanoLund, Lund University, 22100 Lund, Sweden*

(Received 6 April 2022; revised 20 January 2023; accepted 27 January 2023; published 13 February 2023)

We report supercurrent transport measurements in hybrid Josephson junctions comprising semiconducting InAs nanowires with epitaxial ferromagnetic insulator EuS and superconducting Al coatings. The wires display a hysteretic superconducting window close to the coercivity, away from zero external magnetic field. Using a multi-interferometer setup, we measure the current-phase relation of multiple magnetic junctions and find an abrupt switch between π and 0 phases within the superconducting window. We attribute the 0-π transition to the discrete flipping of the EuS domains and provide a qualitative theory showing that a sizable exchange field can polarize the junction and lead to the supercurrent reversal. Both 0 and π phases can be realized at zero external field by demagnetizing the wire.

DOI: 10.1103/PhysRevB.107.L081301

Unexpected quantum behavior often appears in hybrid devices made from materials with competing electrical properties [1–3]. For instance, Josephson junctions with ferromagnetic barriers can develop a superconducting phase difference of π giving rise to supercurrent reversal [4,5] and spontaneous currents in superconducting loops [6]. The superconducting phase shift in metallic samples typically originates from the oscillatory damping of the pairing amplitude in the junction [7,8]. However, it can also arise from spin-flip scattering via magnetic impurities [9,10] or an alternating magnetization in multidomain junctions [11]. The dependence of the superconducting parameters on the magnetic domain structure has been investigated in samples with metallic [12] and insulating [13,14] ferromagnetic components, but the impact of domain configuration on the π-junction formation remains largely unexplored.

Spin-active scattering at an interface between a superconductor and a ferromagnetic insulator can induce a Zeeman-like splitting [15,16] and give rise to spin-polarized Andreev bound states (ABSs) [17]. Superconducting junctions with large interfacial exchange interactions are predicted to develop a π phase shift [18–20] with intrinsically low quasiparticle dissipation [21,22], making them attractive for both classical and quantum applications [23–25]. Previously, supercurrent transport through spin-dependent barriers showed signatures of unconventional superconductivity [26] and an incomplete 0-π transition [27] associated with the multidomain structure in the junction.

An alternative route to Josephson π junctions is to couple a semiconducting quantum dot [28–30] or superconducting hybrid island [31,32] to superconducting leads, where adding or removing a single electron spin can result in a supercurrent reversal. The transition between the 0 and π phases in such junctions can be controlled electrostatically [33–35] or by an external magnetic field [36,37]. Recently developed semiconducting InAs nanowires with epitaxial superconducting Al and ferromagnetic insulator EuS shells [38–40] showed the coexistence of induced superconductivity and ferromagnetism, and signatures of spin-polarized bound states [41,42]. The latter were investigated theoretically in the context of topological superconductivity [43–50]. Here, we study triple-hybrid Josephson junctions containing components of spin-dependent transport and gate-voltage controlled barriers.

To demonstrate the emergence of π junctions in ferromagnetic hybrid nanowires, we studied a multi-interferometer device consisting of ferromagnetic (target) and nonmagnetic (reference) wires. The two wires, denoted A and B, were placed next to each other on a Si substrate with 200-nm SiO_x capping. The middle and the ends of both wires were connected by *ex situ* Al contacts, forming multiple loops [Fig. 1(a)]. The main wire A comprised a hexagonal InAs core with epitaxial two-facet EuS and three-facet *in situ* Al shells, with the Al fully covering both EuS facets and one InAs facet. The reference wire B with an InAs core and three-facet Al shell did not include EuS. Four junctions, denoted j_1^F, j_2^F on the ferromagnetic wire A, and j_3, j_4 on the reference wire B, were formed by selectively removing ~100 nm of *in situ* Al in the segments between the Ohmic contacts. Top gates were fabricated over all four junctions after the deposition of a thin HfO_x dielectric layer, allowing independent electrostatic control of each junction.

The phase across a particular junction relative to a reference junction was measured by depleting the other two junctions, thus forming a single superconducting interferometer. Three triple-hybrid junctions, from two different devices, were investigated and showed similar results. We report data

*These authors contributed equally to this work.
†Present address: Department of Electrical, Computer & Energy Engineering, University of Colorado, Boulder, Colorado 80309, USA.

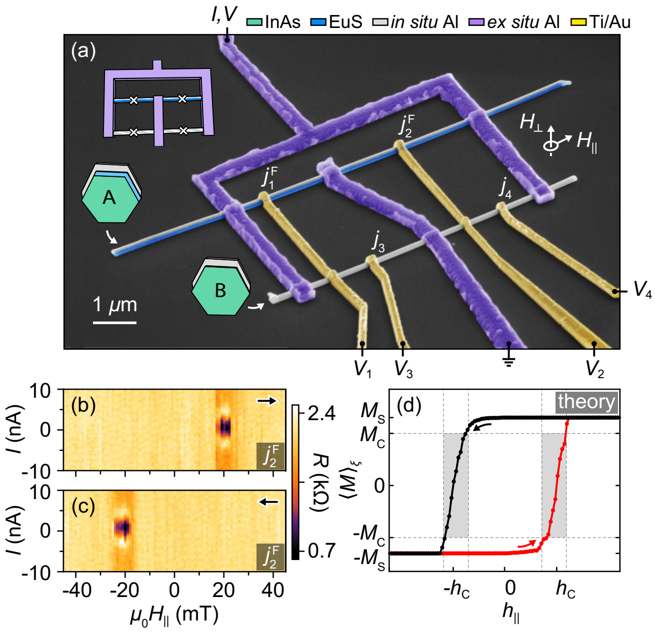

FIG. 1. (a) Color-enhanced micrograph of a representative multi-interferometer device comprising ferromagnetic (target) and non-magnetic (reference) nanowires. The insets show the schematic device layout and wire cross sections. (b) and (c) Differential resistance R as a function of current bias I and parallel external magnetic field $H_\parallel$ measured for the j_2^F junction sweeping $H_\parallel$ from (b) negative to positive and (c) positive to negative. R is suppressed in a narrow, sweep-direction-dependent window away from $H_\parallel = 0$. (d) Disorder-averaged induced magnetization $\langle M \rangle_\xi$ calculated using the random-field Ising model. $h_\parallel$ is a model parameter representing an external magnetic field. The junction superconducts only in a narrow hysteretic window (gray) around the coercive field $\pm h_C$ and is otherwise normal.

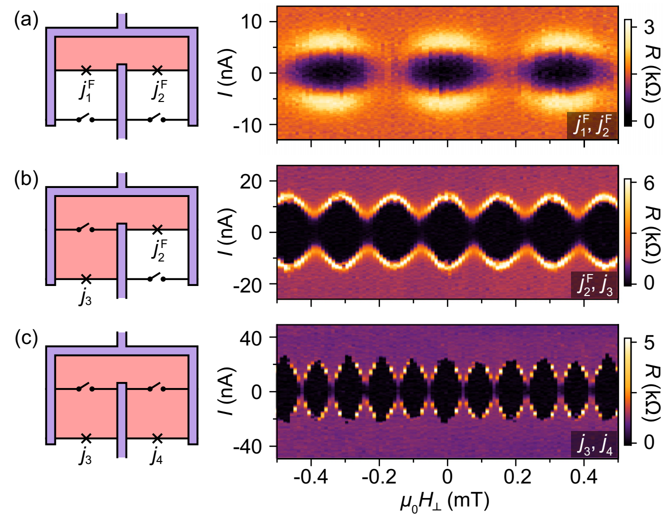

FIG. 2. Left panels: Schematics of the multi-interferometer device in various open and closed junction configurations with highlighted effective loop areas. Right panels: Corresponding current-phase relations represented by differential resistance R measured as a function of current bias I and flux-threading perpendicular magnetic field $H_\perp$ for (a) two ferromagnetic, (b) one ferromagnetic and one nonmagnetic, and (c) two nonmagnetic junctions. All junction configurations show effective-area-dependent, periodic switching current modulations in $H_\perp$.

from a representative junction in the main text and present supporting data from the other two junctions in the Supplemental Material [51]. Measurements were carried out using standard ac lock-in techniques in a dilution refrigerator with a three-axis vector magnet and base temperature of 20 mK.

We begin by exploring the magnetotransport properties of a single ferromagnetic junction j_2^F while keeping the other junctions depleted. Four-terminal differential resistance, $R = dV/dI$, of the junction was measured as a function of current bias I and external magnetic field $H_\parallel$ applied parallel to wire A [Figs. 1(b) and 1(c)]. Sweeping from negative to positive field, $R(I)$ remains finite and featureless throughout the measured range, except between $\mu_0 H_\parallel = 15$ and 25 mT, where $R(I)$ decreases abruptly for $|I| \lesssim 5$ nA [Fig. 1(b)]. Reversing the sweep direction of $H_\parallel$ shifts the low-resistance window to around -20 mT [Fig. 1(c)]. A similar hysteretic dip in resistance has been reported in uninterrupted EuS/Al bilayer films [52].

We interpret the observed behavior as the recovery of the superconductivity near the coercive field H_C, where the induced magnetization $\langle M \rangle_\xi$ averaged over the superconducting coherence length ξ decreases below a critical value M_C. To verify this picture, we calculate disorder-averaged $\langle M \rangle_\xi$ using the kinetic random-field Ising model (see Supplemental Material [51] and Refs. [53,54] therein). The resulting hysteresis curves [see Fig. 1(d)] are asymmetric around the coercive field. In this regime the EuS domain size is shorter than ξ, which leads to a reduced $\langle M \rangle_\xi$ compared to the saturation value M_S (see Supplemental Material [51] and Refs. [55–60] therein). Realistic hysteresis curves are typically not as smooth as depicted in Fig. 1(d); instead, they display irreversible jumps between discrete magnetization values [41,61,62].

We note that the magnetic junctions in the superconducting state display residual resistance at $I = 0$, which we tentatively attribute to the supercurrent suppression due to the uncertainty in the phase difference across a junction with low Josephson energy [63]. Such phase diffusion can be stabilized by integrating the junction into a superconducting loop [64].

Having established the magnetic-field response of an individual magnetic junction, we next examine the current-phase relations (CPRs) of various junction pairs. To ensure that wire A was superconducting, $\mu_0 H_\parallel$ was first ramped to -100 mT and then tuned to 21 mT, close to H_C, where $R(I \sim 0)$ is suppressed. Three example measurements of distinct superconducting interferometers, formed by opening either two ferromagnetic, mixed, or nonmagnetic junctions, are displayed in Fig. 2. In all three configurations, the device shows periodic switching current I_{SW}, and modulations as a function of the flux-threading perpendicular magnetic field $H_\perp$. The oscillation period changes for different junction combinations due to the different effective loop areas, corresponding to the superconducting flux quantum, $\Phi_0 = h/2e$ (Fig. S1 in Supplemental Material [51]). The zero-flux offset of the magnet was calibrated using the CPR of the loop with two nonmagnetic junctions (j_3 and j_4).

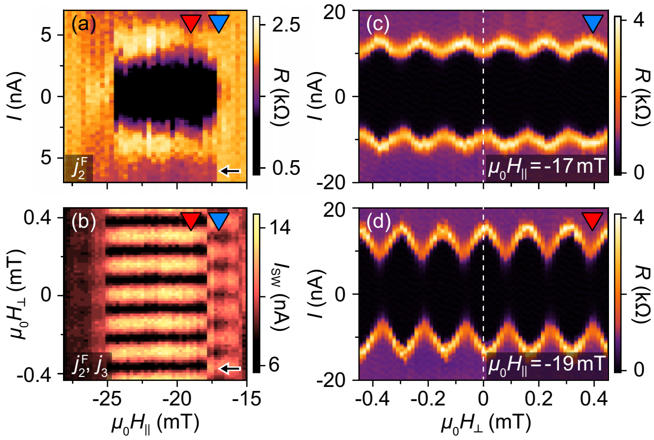

FIG. 3. (a) Differential resistance R of $j_2^{\rm F}$ as a function of current bias I and parallel external magnetic field $H_\parallel$ showing the superconducting window of the junction centered around -21 mT. The data were taken with $j_1^{\rm F}$, j_3, and j_4 depleted. (b) Switching current $I_{\rm SW}$ as a function of flux-threading perpendicular magnetic field $H_\perp$ measured for the $j_2^{\rm F}$-j_3 interferometer at decreasing $H_\parallel$ values. The magnetic junction switches abruptly from the π to 0 phase around -18 mT as $H_\parallel$ is lowered. (c) Current-phase relation measured at $\mu_0 H_\parallel = -17$ mT exhibits $I_{\rm SW}$ minimum at $H_\perp = 0$, suggesting a π junction. (d) Similar to (c) but in the 0-junction regime at $\mu_0 H_\parallel = -19$ mT. All the data were taken after polarizing the wire at $\mu_0 H_\parallel = 100$ mT.

At $\mu_0 H_\parallel = 21$ mT, $I_{\rm SW}$ is maximal at zero flux ($H_\perp = 0$) for all configurations, indicating a homogeneous superconducting phase across the device. However, we find that the loops with magnetic junctions show characteristic π-shifted CPRs at the onset of the superconducting window, before $H_{\rm C}$ is reached (Fig. 3). We study the transition between the two regimes in $j_2^{\rm F}$ by measuring CPRs (using j_3 as a reference, while keeping $j_1^{\rm F}$ and j_4 depleted) over a range of $H_\parallel$ spanning the superconducting window [Fig. 3(a)]. The deduced evolution of $I_{\rm SW}$ with $H_\perp$ and $H_\parallel$ is shown in Fig. 3(b). Outside the superconducting window, $I_{\rm SW}$ is independent of $H_\perp$, indicating that $j_2^{\rm F}$ is not superconducting (Fig. S2 in Supplemental Material [51]). Moving to more negative $H_\parallel$, $j_2^{\rm F}$ displays a π-shifted CPR in the range between -16 and -18 mT [Fig. 3(c)], but then switches abruptly to a state without a phase shift [Fig. 3(d)]. The average $I_{\rm SW}$ is $\sim$10 nA in both cases, but its modulation amplitude increases from around 3 to 6 nA as the CPR phase switches from π to 0 [see Figs. 3(c) and 3(d)]. The superconducting phase remains unchanged throughout the rest of the superconducting window, whereas the amplitude of $I_{\rm SW}$ oscillations shrinks abruptly at -25 mT and once again at -26 mT as the supercurrent through $j_2^{\rm F}$ gets suppressed. This is likely because of the sweep-direction-dependent, discrete jumps of $\langle M \rangle_\xi$ through $M_{\rm C}$ (see Supplemental Material [51]). The transition features were qualitatively the same around positive $H_{\rm C}$, after reversing $H_\parallel$ direction, and did not depend on the gate voltages V_2 and V_3 (see Figs. S3–S5 in Supplemental Material [51]). The transition-field value shifted by a fraction of a millitesla between different runs, presumably due to the magnetic noise from the stochastic domain switching [65]. Furthermore, the superconducting phase shift of π within the superconducting window was observed also for the other two measured ferromagnetic junctions, with $j_1^{\rm F}$ showing hints of a second 0-π transition at the end of its superconducting window (see Figs. S6 and S7).

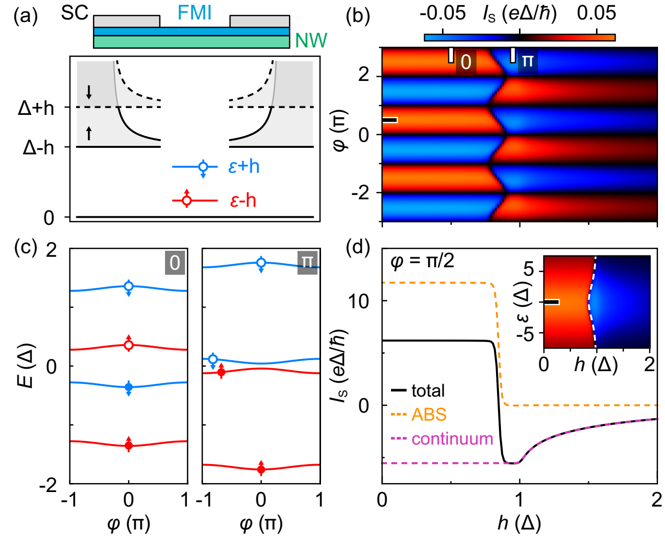

FIG. 4. (a) Schematic illustration of the modeled junction and the corresponding density of states with the induced superconducting gap in the wire leads Δ and a discrete state in the junction at energy ε, both spin split by an exchange field h. (b) Calculated supercurrent $I_{\rm S}$ as a function of the superconducting phase difference across the junction φ and h, showing a 0-π transition for $h \lesssim \Delta$. (c) Energy of Andreev bound states (ABSs) in the junction as a function of φ in the 0 (left) and the π (right) regimes. (d) ABS and continuum contributions to the total $I_{\rm S}$ as a function of h at $\varphi = \pi/2$ and $\varepsilon = 0$. The two contributions have opposite signs for $h \lesssim \Delta$, while the ABS contribution vanishes in the π phase. Inset: $I_{\rm S}$ dependence on ε, where the white line is an analytic expression for the 0-π transition given in the Supplemental Material [51].

These experimental observations suggest that the 0-π transition is driven by a discrete flipping of the EuS domains affecting $\langle M \rangle_\xi$ and changing the effective spin splitting of the ABSs in the junction. We propose a simple transport model demonstrating that a sizable exchange field, arising from $\langle M \rangle_\xi$, can polarize the junction, resulting in the π phase shift. The model describes a nanowire proximity-coupled to a ferromagnetic insulator and an interrupted superconductor, forming a Josephson junction [Fig. 4(a)]. The magnetic insulator induces an exchange field with amplitude $h(x)$, where x is the position along the wire. The superconductor induces a pairing potential, $\Delta(x) = |\Delta| e^{\pm i\varphi/2}$, in the lateral wire regions defining the leads, where φ denotes the superconducting phase difference across the junction. Assuming the short-junction limit, we describe the coupling between the leads by a single state, whose two spin-split levels are at energies $\varepsilon \pm h$. The extension to the long-junction limit including spin-orbit coupling yields qualitatively similar results and is discussed in Ref. [66].

We calculate the supercurrent through the junction $I_{\rm S}$, proportional to $I_{\rm SW}$, using the Green's function formalism (see Supplemental Material [51]). In the tunneling regime, $I_{\rm S}$ displays a π phase shift for $h \lesssim \Delta$ [Fig. 4(b)]. The supercurrent

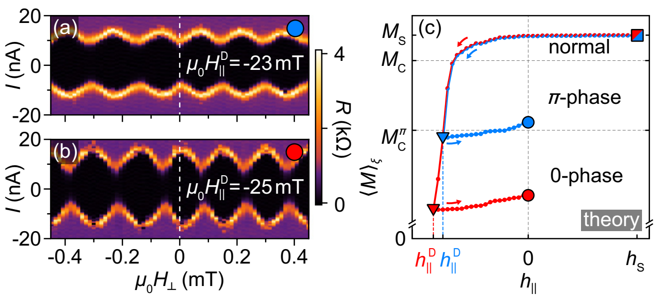

FIG. 5. (a) Differential resistance R as a function of current bias I and flux-threading magnetic field $H_\perp$ measured for a j_2^F-j_3 interferometer at zero parallel external field ($H_\parallel = 0$) showing a π-shifted current-phase relation. The data were taken after polarizing the wire at $\mu_0 H_S = 100$ mT and demagnetizing it at $\mu_0 H_\parallel^D = -23$ mT. (b) Similar to (a) but taken after demagnetizing the wire at $\mu_0 H_\parallel^D = -25$ mT, showing 0-junction behavior. (c) Calculated disorder-averaged induced magnetization $\langle M \rangle_\xi$ illustrating the experimental demagnetization scheme. After saturating $\langle M \rangle_\xi$, the parameter representing the external magnetic field $h_\parallel$ is swept to the variable demagnetization value $h_\parallel^D$, and then back to 0. Depending on $h_\parallel^D$, the junction can either relax to the π or 0 phase.

reversal can be understood by considering the field evolution of ABSs in the junction [Fig. 4(c)]. A finite h lifts the spin degeneracy of the ABSs. For large h, one ABS can cross zero energy, thus changing the junction ground state from an antialigned to an aligned spin configuration. As a result, the ABS contribution to the supercurrent is suppressed, leaving only the subdominant transport via the continuum states with lower magnitude and opposite sign [Fig. 4(d)]. This can be understood by noting that the Josephson current is proportional to the product of the energy-dependent superconducting pairing in the leads $\sim\Delta^2/(\Delta^2 - E^2)$, which becomes negative for energies $E > \Delta$ [67]. In the experiment, the discrete domain flips lead to discontinuous jumps in the phase diagram.

In case of a single barrier in a tunneling regime, the field value of the 0-π transition shows a relatively weak dependence on φ and ε [see Fig. 4(b) and the inset in Fig. 4(d)]. This is distinct from the interaction-driven supercurrent reversal in the quantum-dot regime [29,33,68,69], where the transition can be smoothly tuned by an electrostatic gate changing the occupancy of the junction. The quantum-dot scenario can be excluded since the π phase shows no dependence on the junction-gate voltage (see Fig. S5 in Supplemental Material [51]). Increasing the coupling rates to the leads results in a skewed CPR and a larger h range where 0 and π phases coexist (see Supplemental Material [51]).

Finally, we demonstrate experimentally that the π phase can be realized at zero external magnetic field by demagnetizing EuS with the following procedure (Fig. 5). First, a saturating magnetic field, $\mu_0 H_S = +100$ mT, was applied to fully polarize the EuS. The field was then gradually swept through zero to a demagnetizing (negative) value $H_\parallel^D$ before returning to zero. Carrying out the demagnetization loop for different $H_\parallel^D$ values, we find that j_2^F transitions from a π to 0 phase as $\mu_0 H_\parallel^D$ is changed from -23 to -25 mT [Figs. 5(a) and 5(b), and S8 in Supplemental Material [51]]. This is similar to the behavior observed at the finite external field (Fig. 3), but now measured at $H_\parallel = 0$. Qualitatively the same phenomenology was observed for j_1^F (see Fig. S9 in Supplemental Material [51]). We ascribe this behavior to the $H_\parallel$-controlled EuS domain relaxation into a configuration with the remanent $\langle M \rangle_\xi < M_C$ as $H_\parallel$ is ramped back and forth. The calculated demagnetization loops for two different demagnetization values support this picture [Fig. 5(c)].

In summary, we have studied the current-phase relation of triple-hybrid Josephson junctions comprising semiconducting (InAs) nanowires with epitaxial ferromagnetic insulator (EuS) and superconductor (Al) shells. The magnetic junctions showed a 0-π phase transition within a hysteretic superconducting window in the parallel magnetic field. We interpret the results in the context of magnetic domains and provide a simple theoretical model demonstrating that an induced average magnetization can account for the transition. By demagnetizing the EuS layer, the π phase can be realized at zero magnetic field, making the triple-hybrid junctions an attractive component for quantum and classical applications in superconducting circuitry.

We thank Karsten Flensberg, Martin Leijnse, and Gorm Steffensen for valuable discussions, Claus Sørensen for contributions to materials growth, and Shivendra Upadhyay for assistance with nanofabrication. We acknowledge support from the Danish National Research Foundation, the Danish Council for Independent Research | Natural Sciences, European Research Council (Grants Agreement No. 716655 and No. 856526), Microsoft, NanoLund, and a research grant (Project 43951) from VILLUM FONDEN.

[1] R. Meservey and P. Tedrow, Phys. Rep. **238**, 173 (1994).
[2] F. S. Bergeret, M. Silaev, P. Virtanen, and T. T. Heikkilä, Rev. Mod. Phys. **90**, 041001 (2018).
[3] E. Prada, P. San-Jose, M. W. de Moor, A. Geresdi, E. J. Lee, J. Klinovaja, D. Loss, J. Nygård, R. Aguado, and L. P. Kouwenhoven, Nat. Rev. Phys. **2**, 575 (2020).
[4] V. V. Ryazanov, V. A. Oboznov, A. Y. Rusanov, A. V. Veretennikov, A. A. Golubov, and J. Aarts, Phys. Rev. Lett. **86**, 2427 (2001).
[5] T. Kontos, M. Aprili, J. Lesueur, F. Genêt, B. Stephanidis, and R. Boursier, Phys. Rev. Lett. **89**, 137007 (2002).
[6] A. Bauer, J. Bentner, M. Aprili, M. L. Della Rocca, M. Reinwald, W. Wegscheider, and C. Strunk, Phys. Rev. Lett. **92**, 217001 (2004).
[7] A. I. Buzdin, Rev. Mod. Phys. **77**, 935 (2005).
[8] F. S. Bergeret, A. F. Volkov, and K. B. Efetov, Rev. Mod. Phys. **77**, 1321 (2005).
[9] L. N. Bulaevskii, V. V. Kuzii, and A. A. Sobyanin, Pis'ma Zh. Eksp. Teor. Fiz. **25**, 314 (1977) [JETP Lett. **25**, 290 (1977)].
[10] C. Schrade, A. A. Zyuzin, J. Klinovaja, and D. Loss, Phys. Rev. Lett. **115**, 237001 (2015).

[11] A. F. Volkov and A. Anishchanka, Phys. Rev. B **71**, 024501 (2005).
[12] Z. Yang, M. Lange, A. Volodin, R. Szymczak, and V. V. Moshchalkov, Nat. Mater. **3**, 793 (2004).
[13] E. Strambini, V. N. Golovach, G. De Simoni, J. S. Moodera, F. S. Bergeret, and F. Giazotto, Phys. Rev. Mater. **1**, 054402 (2017).
[14] S. Diesch, P. Machon, M. Wolz, C. Sürgers, D. Beckmann, W. Belzig, and E. Scheer, Nat. Commun. **9**, 5248 (2018).
[15] T. Tokuyasu, J. A. Sauls, and D. Rainer, Phys. Rev. B **38**, 8823 (1988).
[16] X. Hao, J. S. Moodera, and R. Meservey, Phys. Rev. B **42**, 8235 (1990).
[17] D. Beckmann, F. Hübler, M. Wolf, and H. v. Löhneysen, Philos. Trans. R. Soc. A **376**, 20150002 (2018).
[18] Y. Tanaka and S. Kashiwaya, Physica C **274**, 357 (1997).
[19] M. Fogelström, Phys. Rev. B **62**, 11812 (2000).
[20] M. Minutillo, R. Capecelatro, and P. Lucignano, Phys. Rev. B **104**, 184504 (2021).
[21] S. Kawabata, S. Kashiwaya, Y. Asano, Y. Tanaka, and A. A. Golubov, Phys. Rev. B **74**, 180502(R) (2006).
[22] T. Kato, A. A. Golubov, and Y. Nakamura, Phys. Rev. B **76**, 172502 (2007).
[23] L. B. Ioffe, V. B. Geshkenbein, M. V. Feigel'man, A. L. Fauchere, and G. Blatter, Nature (London) **398**, 679 (1999).
[24] A. Feofanov, V. Oboznov, V. Bol'ginov, J. Lisenfeld, S. Poletto, V. Ryazanov, A. Rossolenko, M. Khabipov, D. Balashov, A. Zorin *et al.*, Nat. Phys. **6**, 593 (2010).
[25] E. Gingrich, B. M. Niedzielski, J. A. Glick, Y. Wang, D. Miller, R. Loloee, W. Pratt, Jr., and N. O. Birge, Nat. Phys. **12**, 564 (2016).
[26] K. Senapati, M. G. Blamire, and Z. H. Barber, Nat. Mater. **10**, 849 (2011).
[27] R. Caruso, D. Massarotti, G. Campagnano, A. Pal, H. G. Ahmad, P. Lucignano, M. Eschrig, M. G. Blamire, and F. Tafuri, Phys. Rev. Lett. **122**, 047002 (2019).
[28] B. I. Spivak and S. A. Kivelson, Phys. Rev. B **43**, 3740 (1991).
[29] J. A. van Dam, Y. V. Nazarov, E. P. Bakkers, S. De Franceschi, and L. P. Kouwenhoven, Nature (London) **442**, 667 (2006).
[30] D. Bouman, R. J. J. van Gulik, G. Steffensen, D. Pataki, P. Boross, P. Krogstrup, J. Nygård, J. Paaske, A. Pályi, and A. Geresdi, Phys. Rev. B **102**, 220505(R) (2020).
[31] C. Schrade and L. Fu, Phys. Rev. Lett. **120**, 267002 (2018).
[32] J.-Y. Wang, C. Schrade, V. Levajac, D. van Driel, K. Li, S. Gazibegovic, G. Badawy, R. L. Op het Veld, J. S. Lee, M. Pendharkar, C. P. Dempsey, C. J. Palmstrom, E. P. Bakkers, L. Fu, L. P. Kouwenhoven, and J. Shen, Sci. Adv. **8**, eabm9896 (2022).
[33] D. Razmadze, E. C. T. O'Farrell, P. Krogstrup, and C. M. Marcus, Phys. Rev. Lett. **125**, 116803 (2020).
[34] O. A. Awoga, J. Cayao, and A. M. Black-Schaffer, Phys. Rev. Lett. **123**, 117001 (2019).
[35] J. Schulenborg and K. Flensberg, Phys. Rev. B **101**, 014512 (2020).
[36] A. M. Whiticar, A. Fornieri, A. Banerjee, A. C. C. Drachmann, S. Gronin, G. C. Gardner, T. Lindemann, M. J. Manfra, and C. M. Marcus, Phys. Rev. B **103**, 245308 (2021).
[37] A. Bargerbos, M. Pita-Vidal, R. Žitko, J. Ávila, L. J. Splitthoff, L. Grünhaupt, J. J. Wesdorp, C. K. Andersen, Y. Liu, L. P. Kouwenhoven, R. Aguado, A. Kou, and B. van Heck, PRX Quantum **3**, 030311 (2022).
[38] P. Krogstrup, N. Ziino, W. Chang, S. Albrecht, M. Madsen, E. Johnson, J. Nygård, C. Marcus, and T. Jespersen, Nat. Mater. **14**, 400 (2015).
[39] Y. Liu, A. Luchini, S. Martí-Sánchez, C. Koch, S. Schuwalow, S. A. Khan, T. Stankevič, S. Francoual, J. R. Mardegan, J. Krieger, V. N. Strocov, J. Stahn, C. A. F. Vaz, M. Ramakrishnan, U. Staub, K. Lefmann, G. Aeppli, J. Arbiol, and P. Krogstrup, ACS Appl. Mater. Interfaces **12**, 8780 (2020).
[40] Y. Liu, S. Vaitiekėnas, S. Marti-Sanchez, C. Koch, S. Hart, Z. Cui, T. Kanne, S. A. Khan, R. Tanta, S. Upadhyay, M. Espineira Cachaza, C. M. Marcus, J. Arbiol, K. A. Moler, and P. Krogstrup, Nano Lett. **20**, 456 (2020).
[41] S. Vaitiekėnas, Y. Liu, P. Krogstrup, and C. Marcus, Nat. Phys. **17**, 43 (2021).
[42] S. Vaitiekėnas, R. S. Souto, Y. Liu, P. Krogstrup, K. Flensberg, M. Leijnse, and C. M. Marcus, Phys. Rev. B **105**, L041304 (2022).
[43] B. D. Woods and T. D. Stanescu, Phys. Rev. B **104**, 195433 (2021).
[44] A. Maiani, R. Seoane Souto, M. Leijnse, and K. Flensberg, Phys. Rev. B **103**, 104508 (2021).
[45] S. D. Escribano, E. Prada, Y. Oreg, and A. L. Yeyati, Phys. Rev. B **104**, L041404 (2021).
[46] C.-X. Liu, S. Schuwalow, Y. Liu, K. Vilkelis, A. L. R. Manesco, P. Krogstrup, and M. Wimmer, Phys. Rev. B **104**, 014516 (2021).
[47] J. Langbehn, S. Acero González, P. W. Brouwer, and F. von Oppen, Phys. Rev. B **103**, 165301 (2021).
[48] A. Khindanov, J. Alicea, P. Lee, W. S. Cole, and A. E. Antipov, Phys. Rev. B **103**, 134506 (2021).
[49] C.-X. Liu and M. Wimmer, Phys. Rev. B **105**, 224502 (2022).
[50] S. D. Escribano, A. Maiani, M. Leijnse, K. Flensberg, Y. Oreg, A. L. Yeyati, E. Prada, and R. S. Souto, npj Quantum Mater. **7**, 81 (2022).
[51] See Supplemental Material at http://link.aps.org/supplemental/10.1103/PhysRevB.107.L081301 for sample preparation and measurement details, theoretical model description, and additional data.
[52] B. Li, N. Roschewsky, B. A. Assaf, M. Eich, M. Epstein-Martin, D. Heiman, M. Münzenberg, and J. S. Moodera, Phys. Rev. Lett. **110**, 097001 (2013).
[53] J. P. Sethna, K. Dahmen, S. Kartha, J. A. Krumhansl, B. W. Roberts, and J. D. Shore, Phys. Rev. Lett. **70**, 3347 (1993).
[54] R. J. Glauber, J. Math. Phys. **4**, 294 (1963).
[55] C. Kittel, *Introduction to Solid State Physics*, 8th ed. (Wiley, New York, 2005).
[56] M. Tinkham, *Introduction to Superconductivity*, 2nd ed. (McGraw-Hill, New York, 1996).
[57] S. Vaitiekėnas, P. Krogstrup, and C. Marcus, Phys. Rev. B **101**, 060507 (2020).
[58] R. C. Bruno and B. B. Schwartz, Phys. Rev. B **8**, 3161 (1973).
[59] B. S. Chandrasekhar, Appl. Phys. Lett. **1**, 7 (1962).
[60] A. M. Clogston, Phys. Rev. Lett. **9**, 266 (1962).
[61] M. J. Wolf, C. Sürgers, G. Fischer, and D. Beckmann, Phys. Rev. B **90**, 144509 (2014).
[62] A. Hijano, S. Ilić, M. Rouco, C. González-Orellana, M. Ilyn, C. Rogero, P. Virtanen, T. T. Heikkilä, S. Khorshidian, M. Spies,

N. Ligato, F. Giazotto, E. Strambini, and F. S. Bergeret, Phys. Rev. Res. **3**, 023131 (2021).
[63] W.-S. Lu, K. Kalashnikov, P. Kamenov, T. J. DiNapoli, and M. E. Gershenson, Electronics **12**, 416 (2023).
[64] D. Sullivan, S. Dutta, M. Dreyer, M. Gubrud, A. Roychowdhury, J. Anderson, C. Lobb, and F. Wellstood, J. Appl. Phys. **113**, 183905 (2013).
[65] E. Puppin, Phys. Rev. Lett. **84**, 5415 (2000).
[66] A. Maiani, K. Flensberg, M. Leijnse, C. Schrade, S. Vaitiekėnas, and R. Seoane Souto, arXiv:2302.04267.
[67] A. Martín-Rodero and A. L. Yeyati, Adv. Phys. **60**, 899 (2011).
[68] R. Delagrange, R. Weil, A. Kasumov, M. Ferrier, H. Bouchiat, and R. Deblock, Phys. Rev. B **93**, 195437 (2016).
[69] A. V. Rozhkov, T. Liu, A. V. Andreev, and B. Z. Spivak, Phys. Rev. B **105**, L201401 (2022).